Korean J. Chem. Eng., 38(3), 552-564 (2021)
DOI: 10.1007/s11814-020-0715-y

pISSN: 0256-1115
eISSN: 1975-7220

Numerical investigation of the mixing process in a Twin Cam Mixer: Influence of triangular cam height-base ratio and eccentricity

Yu He*,, Xiwen Li*,**, Jiecai Long*,**, Baojun Shen*,**, Zhibin Sun*,**, Yili Yang*,**, and Xiaobin Zhan*,**,†**

*State Key Laboratory of Digital Manufacturing Equipment and Technology, Huazhong University of Science and Technology, Wuhan 430074, China
**School of Mechanical Science and Engineering, Huazhong University of Science and Technology, Wuhan 430074, China
(*Received 28 July 2020 • Revised 20 October 2020 • Accepted 16 November 2020*)

Abstract−The twin cam mixer (TCM), as a general-purpose mixer, shares many attributes in common with 3D industrial mixers, like the internal mixer. We investigated the mixing process in a 2D TCM with two identical isosceles triangular cams rotating at 0.5 rpm. A 2D numerical model coupled with the species transport model was employed to study the influence of cam height-base ratio and eccentricity qualitatively and quantitatively, and both were found to have a significant effect on the mixing behavior of the mixer. Furthermore, a dimensionless parameter, named the modified pressurization coefficient, is put forward to quantify the geometry of the mixer. The logarithmic relationship between the modified pressurization coefficient and the mixing quality was discovered and expected to provide new ideas for establishing the relationship between the geometric parameters of a mixer and its mixing performance.

Keywords: Twin Cam Mixer, Mixing Process, 2D Numerical Model, Species Transport, Pressurization Coefficient

INTRODUCTION

Mixing is a common process in fields such as pharmaceutical, chemical and food processing. Whereas the quality of mixing is fundamental to guarantee the desired properties of products [1], much research effort has been devoted to describing and understanding the mixing process for several decades. During the mixing process, the fluid flow can be distinguished to laminar flow, transition flow, and turbulent flow based on the Reynolds number (*Re*). For the mixing of highly viscous materials (e.g., dough, plastic and rubber), which is dominated by the laminar flow, mixers with the ability to generate vigorous advection are necessary.

So far, many mixing devices have been designed, which can be divided into two categories: dynamic and static. One of the most common static mixers is the tubular flow reactor where liquid is mixed owing to the turbulent character of a liquid flux fed into it [2]. However, dynamic mixers are more widely used in industry and come in many varieties, such as vibromixers (mixers with reciprocating discs) [3], agitated vessels with rotational impellers, and rotor-stator mixers [4]. The twin cam mixer (TCM) belongs to rotor-stator mixers and is equipped with two cams as rotors. The liquid inside a TCM is mixed mainly due to the property of stretch and fold, which makes TCM suitable for mixing highly viscous materials. Furthermore, TCM is a general-purpose mixer that shares many attributes in common with 3D industrial mixers [5]. It is comparable to a 2D cross-section of internal mixer and twin screw extruder (TSE), which are both commonly used for processing highly viscous materials. Therefore, a substantial amount of investigation on TCM has been conducted. Avalosse and Crochet [6] first studied a TCM equipped with equilateral triangular cams experimentally and numerically. Their numerical results exhibited a good correspondence with the experimental counterpart. The flow in an identical TCM was also simulated by Bertrand et al. [7], employing a fictitious domain method and a mesh refinement technique. To analyze the mixing in the TCM, Robinson et al. [8] and Eitzlmayr et al. [9] presented a Lagrangian method called smoothed particle hydrodynamics (SPH). With the method, Robinson et al. [5] explored the influence of cam geometry and operating conditions on the mixing in the TCM. It is noteworthy that when studying the effects of cam geometry, they concentrated on three different geometric variations (see Robinson et al. [5]) instead of building a relationship between a specific geometric parameter and the mixing performance. In addition, Liu et al. [10] and Chen et al. [11] investigated the fluid flow in the mixers comparable to a cross section of TCM. To the best of the authors' knowledge, all the existing research on TCM does not involve cam height-base ratio and eccentricity, and it is for the first time that the effects of the two parameters on the mixing process are considered.

A good understanding about the mixing capability of mixers based on their geometric shapes is important to predict mixing processes and design or optimize mixers [12]. The identification of suitable geometries for mixers to achieve well-mixed products has attracted increasing attention. Thus, a large amount of literature concerning the influence of mixer geometry on mixing performance can be found. For example, Salahudeen et al. [13] and Chen et al. [11] conducted a comparative study of the mixers in terms of rotor cross section. Luo et al. [14] and Xu et al. [15] compared the mixing performance of a non-twin screws extruder (NTSE) with that of a traditional TSE. Apart from rotor cross section, other design variables, e.g., stagger angle [16-18], tip clearance [19] and tip angle

†To whom correspondence should be addressed.
E-mail: zhanxb@hust.edu.cn
Copyright by The Korean Institute of Chemical Engineers.

[20,21], were also investigated by some as the impact factors of mixing process. From these studies, it can be found that the mixing capability of a mixer is largely determined by the geometry of its mixing elements.

To understand the mixing capability of mixers, experimental analyses of the flows in mixers are usually performed with the aid of tracers. Carneiro et al. [22] carried out flow visualization studies on the flow patterns in a TSE through injecting a tracer into the mixing field. Visualization studies were also conducted by Avalosse and Crochet [6] to evaluate the mixing process in a TCM. Some tracers with special properties can be adopted to conduct specific experiments. Zhang et al. [17,23,24] used a fluorescent tracer to measure residence time distribution (RTD) in a TSE. Shearer and Tzoganakis [25-28] adopted a reactive tracer to investigate the distributive mixing in a TSE.

Although the experimental investigation technique is common in evaluating the mixing capability of mixers, it is time-consuming and expensive [29]. In recent years, with the rapid development of the computational technology, numerical simulation has become a powerful tool to get local and detailed information of mixing processes [1,30-32]. For mixers with constant cross sections, a simplified 2D model can be applied to simulate flow in the mixing field owing to similar flow patterns and mixing processes. Connelly et al. [33-35] utilized a 2D finite element method to examine the mixing capability of single- and twin-screw mixers. 2D flow in single- and twin-screw extruders was also simulated by He et al. [36] with a fictitious domain method. Cheng and Manas-Zloczower [37] employed 2D analysis to study the flow patterns in a Banbury mixer. They found that the results of the analysis agreed well with experimental observations. In the numerical study on TCM, Avalosse and Crochet [6] introduced simplifications to reduce actual 3D flow to 2D counterparts, and the numerical results exhibited a good correspondence with their experimental counterpart.

The aim of this paper was to investigate the mixing process of two initially stratified miscible fluids in a 2D TCM with triangular cams rotating at 0.5 rpm. At first, by comparing the simulated mixing process in a TCM with the experimental results from Avalosse and Crochet [6], the 2D numerical model and species transport model were validated. Then, the mixing mechanism in TCM was explained with a selected case. Subsequently, using the two models validated above, the influence of cam height-base ratio and eccentricity on the mixing process was investigated qualitatively and quantitatively. Finally, a dimensionless parameter, namely the modified pressurization coefficient, determined by cam height-base ratio and eccentricity, was proposed to characterize the mixing efficiency in TCM. This paper gives an insight into the mixing process in TCM and provides new ideas for establishing the relationship between the geometric parameters of a mixer and its mixing performance.

NUMERICAL SIMULATION METHODS

1. Mixer Geometry

A schematic of a 2D TCM geometry is shown in Fig. 1, which consists of an 8-shaped cavity formed by two cylinders housing two triangular cams that co-rotate around the two centers of the cylinders (P_{rl} and P_{rr} represent the left and right centers, respectively). The distance (a) between the two centers is 48 mm. The diameters (d) of the cylinders are both 60 mm. The triangular cams considered in this study are isosceles. h and b are the height and base of the cams, respectively. The height-base ratio (r) is defined as the ratio of h to b. As shown in Fig. 1, P_{cl} and P_{cr} represent the centroids of the left and right cams, respectively. The eccentric distance (E) is the distance between the center of the cylinder and the centroid of the cam therein. The eccentricity (e) is defined as the ratio of E to the radius of the cylinder. The (x, y) coordinate system is shown in Fig. 1. The origin of the coordinate system is located at the center of the cavity.

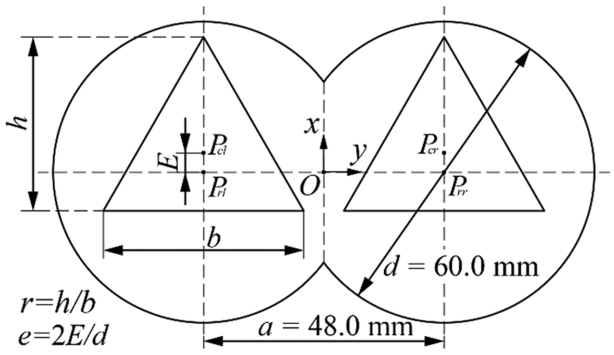


Fig. 1. Schematic of a 2D TCM.

In this paper, the fluid mixing in the 2D TCM as a function of r and e was studied. For the purpose of case study, r and e varied in a certain range without structure interference taking place during the rotation of the cams. To compare the mixing processes fairly, the area of the cams was kept constant so that the area of the fluid domain could remain unchanged. As noted above, isosceles triangular cams are considered here, so the cams can be determined for a given r. The case study with varying r and e is presented in Section MIXING RESULTS.

2. Mathematical Model

In this study, the two-phase miscible, incompressible, and isothermal flow in the 2D TCM was simulated. The flow in the calculation domain was described by the governing equations, including the continuity and momentum, which could be given as: [38]

$$\text{Continuity: } \frac{\partial \rho}{\partial t} + \nabla \cdot \rho \mathbf{u} = 0 \tag{1}$$

$$\text{Momentum: } \frac{\partial}{\partial t}(\rho \mathbf{u}) + \nabla \cdot (\rho \mathbf{u}\mathbf{u}) = -\nabla p + \nabla \cdot \tau + \mathbf{F} \tag{2}$$

where ρ is the fluid density, $\mathbf{u}$ is the velocity vector, p is the fluid pressure, t is time, τ is the viscous stress tensor and $\mathbf{F}$ is the source term.

A species transport model was applied to solve the mass fraction evolution of two miscible fluids in the 2D TCM. The conservation equation of species *i* could be given by: [30]

$$\frac{\partial}{\partial t}(\rho f_i) + \nabla \cdot (\rho f_i \mathbf{u}) = \nabla \cdot (\rho D_m \nabla f_i) \tag{3}$$

where f_i and D_m refer to the local mass fraction of species *i* and the

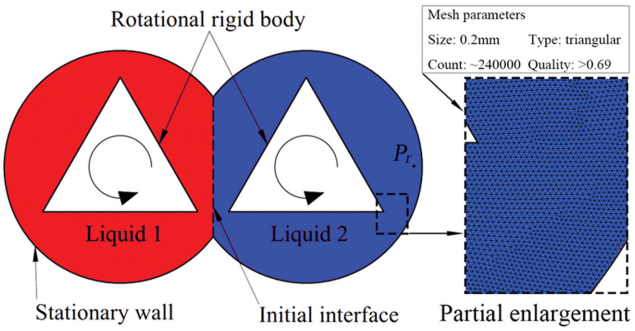


Fig. 2. Initial interface, boundary conditions and meshes of simulations (r=0.866, e=0).

mass diffusion coefficient, respectively.

3. Numerical Details

The two miscible fluids employed by Avalosse and Crochet [6] in their experiment were both aqueous solutions of glucose (with a spot of glucose colored) that was a Newtonian fluid with a viscosity of 50 Pa·s and a density of 1,500 kg/m^3. In this study, the two fluids, Liquid 1 and 2, with identical properties were adopted in all simulations. Liquid 1 and 2 (see Fig. 2) were initially stratified at the interface located along the line x=0 and fully occupied the left and right cylinders, respectively, under the initial conditions. As depicted in Fig. 2, the internal surface of the cavity was set as a stationary no-slip wall boundary. The two cams of the TCM were considered as rotational rigid bodies here and their outside surfaces were defined as moving no-slip walls. Similar settings of boundary conditions can be found in other literature [10,39]. In addition, the two cams co-rotated counter-clockwise at 0.5 rpm, which yielded a Reynolds number on the order of 0.001. Hence, the laminar model was used to simulate the flow field in the TCM.

As mentioned above, Liquid 1 and 2 had the same properties; thus a numerical study was conducted based on the following assumptions:

- Chemical reactions did not take place between the two fluids;
- There was no interfacial tension between the fluids;
- Buoyant mixing did not occur due to the same density of the two fluids, and the gravity was ignored here.

In this study, the commercial software ANSYS Fluent 19.0 was employed to solve the above-mentioned equations. In all simulations, the semi-implicit method for pressure linked equations (SIMPLE) algorithm was adopted to couple pressure and velocity. The second-order upwind scheme was used for the spatial discretization of the momentum and species, and the second-order implicit scheme for the transient formulation. The spatial discretization methods of PRESTO and least squares cell based were used for pressure and gradient, respectively. In addition, the time step (Δt) was set to 0.2 s, which corresponded to 0.6° rotation of the cams.

Table 1. Geometric parameters of TCM for the mesh independence study

Parameters	Values
Base, b (mm)	40
Height, h (mm)	~34.64
Height-base ratio, r	~0.866
Eccentricity, e	0
Cam area, S_{cam} (mm^2)	~692.82

4. Mesh Independence Study

In this study, the dynamic mesh scheme is required due to the constantly varying shape of the computational domain. In the dynamic mesh scheme, the re-meshing and smoothing procedures were adopted to update the grids. For smoothing procedure, the Spring method was adopted. The convergence tolerance was set to 0.001 and the maximum iteration per time step was 20. For re-meshing procedure, the methods of local cell and region face were adopted. The threshold of cell skewness was set to 0.6 to avoid excessive deformation of the grid cells. The re-meshing interval was set to 50. According to ANSYS Fluent Users' guide, [40] only triangular mesh can be remeshed by Fluent in 2D simulation. Hence, triangular meshes (see Fig. 2) were adopted for meshing the computational domain.

A mesh independence study was performed using a TCM equipped with equilateral triangular cams. The geometric parameters of the TCM are listed in Table 1. Note that the cam area (S_{cam}) in our work was equal to that of the mesh independence study, that is, approximately 692.82 mm^2. The simulation results with three mesh sizes (Δx), namely 0.1, 0.2, and 0.4 mm, were compared. To reduce the computational cost, the simulations stopped when the revolutions of the cams reached 4, which was sufficient for the mesh independence test. The velocity (u) and mass fraction of Liquid 2

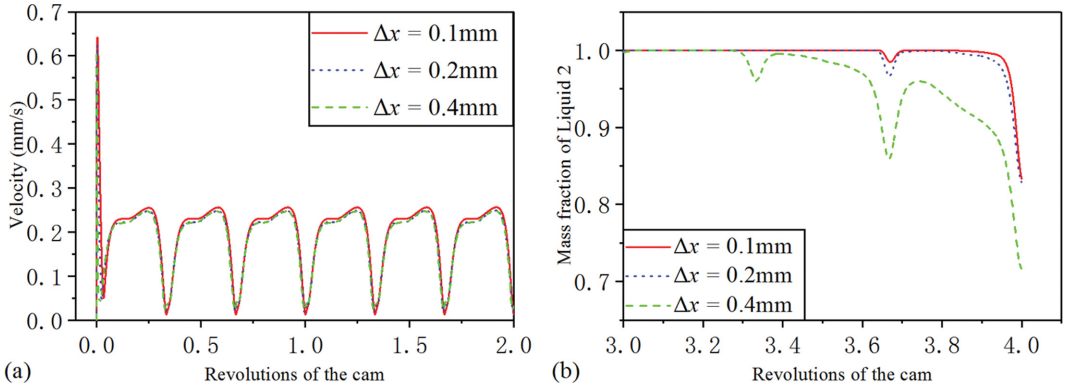


Fig. 3. Variation of velocity (a) and mass fraction of Liquid 2 (b) with respect to the revolutions of the cams (r=0.866, e=0).

Table 2. Computational parameters and costs at N=4 for different cases

Mesh size, Δx (mm)	Time step, Δt (s)	Revolutions of the cam, N	CPU, core count	Computational time (day)
0.1	0.2	4	4	10
0.2	0.2	4	4	3
0.4	0.2	4	4	1

(f_2) were sampled at a point (P_r) located on the right of the right cam (see Fig. 2) corresponding to the coordinates of (0, 52 mm).

Fig. 3 presents the variations of the velocity and mass fraction of Liquid 2 at P_r with respect to the revolutions of the cams (N) obtained with three different mesh sizes. The velocity profiles (see Fig. 3(a)) indicate that the predicted velocity with mesh size Δx of 0.4 mm was already mesh independent, because the results obtained with three mesh sizes almost overlapped. Also, the relatively large initial velocity was due to the unstable initial conditions. Shortly afterwards, the predicted velocity varied periodically with respect to the revolutions of the cams, from which it can be concluded that the change of mesh sizes due to the dynamic mesh scheme has insignificant effect on the simulation results. On the other hand, it can be observed that the results regarding the mass fraction of Liquid 2 obtained with the mesh sizes of 0.1 and 0.2 mm (see Fig. 3(b)) are nearly identical, with an error smaller than 3%, while the results obtained with the mesh size of 0.4 mm have distinct difference from those derived with the mesh size of 0.1 mm, with the maximum error around 16%. Accordingly, the mesh size (Δx) of 0.2 mm was selected to guarantee the accuracy of simulations and reduce the computational cost. The computational costs at N=4 for three cases are listed in Table 2.

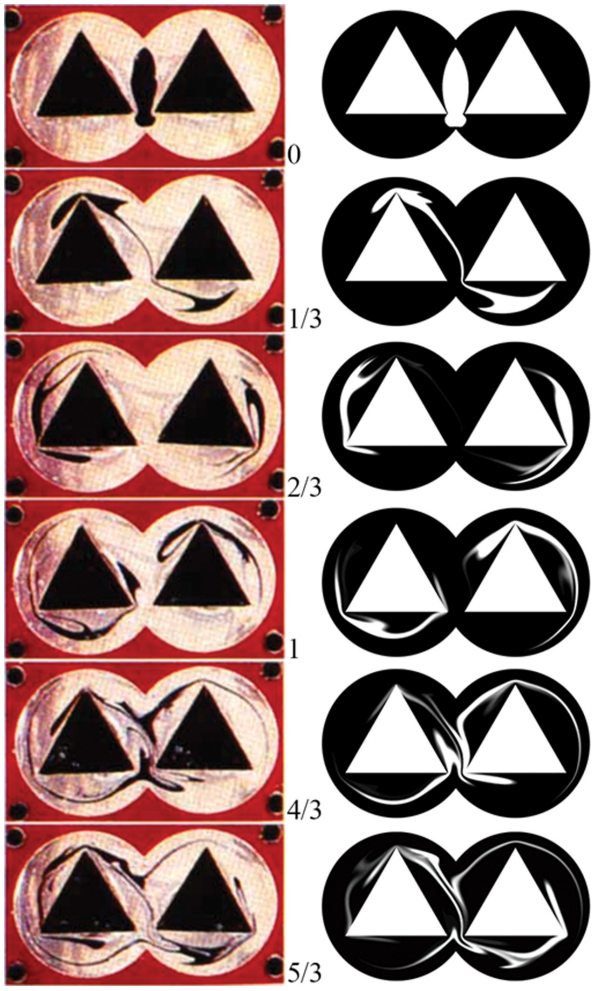


Fig. 4. Comparison of mass fraction contour with experimental snapshots of the tracer by Avalosse and Crochet [6] during the rotation of the triangular cams for 0-5/3 revolutions (r=0.866, e=0).

5. Validation of Numerical Model

To assess the reliability of the present numerical model, the simulated results were qualitatively and quantitatively compared with the work of Avalosse and Crochet [6] in which tracer spreading was observed through visualization experiments at different revolutions of the cams. The same geometric conditions (r=0.866, e=0) and settings as those experimentally undertaken by Avalosse and Crochet [6] were employed. The details on the experiments can refer to the literature. As shown in Fig. 4, the tracer mass fraction contours predicted by the present numerical model (in the right column) and the experimental snapshots from Avalosse and Crochet [6] (in the left column) were compared every 1/3rd revolution of the cams. The comparison proves that the predicted tracer mass fractions are consistent with the tracer patterns for varying revolutions. Moreover, the length of interface between fluids with and without the tracer was adopted for quantitative verification. At

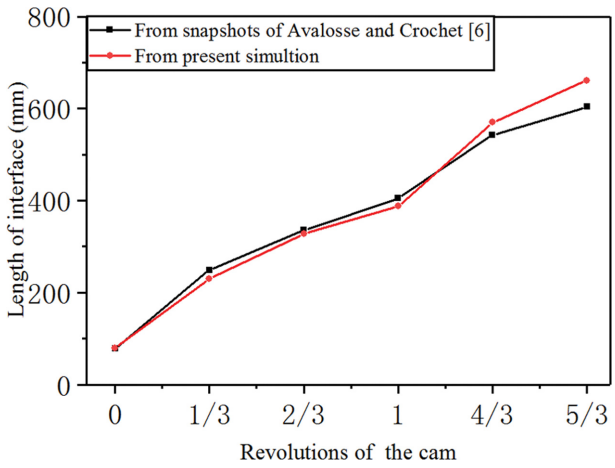


Fig. 5. Comparison between present simulation results and experiment results regarding the length of interface during the rotation of the triangular cams for 0-5/3 revolutions (r=0.866, e=0).

first, the experimental snapshots shown in Fig. 4 were processed to calculate the tracer edge length as the length of interface through the software Matlab. Then, the length of interface from the present simulation was calculated by Fluent. Finally, a quantitative comparison between numerical and experimental results was conducted and shown in Fig. 5. A good agreement with an error smaller than 10% can been found between the two groups of results. In summary, the present numerical model is reliable for studying the mixing process in TCM.

QUANTITATIVE MIXING

For the quantitative assessment on the impact of cam height-base ratio (r) and eccentricity (e) on the mixing process, three dimensionless parameters--the mixing quality (α), the mean mass fraction of Liquid 1 in the left cylinder (f_{lavg}) and the length stretch (β)--were adopted. The mixing quality, a usual parameter to estimate the degree of mixing, [41,42] is defined as:

$$\alpha = 1 - \sqrt{\frac{\sigma^2}{\sigma^2_{max}}} \tag{4}$$

where σ^2 is the variance of mass fraction distribution and σ^2_{max} is the maximum variance. In this study, σ^2_{max} is 0.25 under the symmetrical initial conditions as shown in Fig. 2. In Eq. (4), $\alpha=1$ means that the two fluids are homogeneously mixed, while $\alpha=0$ the two fluids are segregated. The magnitude of the variance of mass fraction distribution (σ^2) can be calculated by solving the mean squared difference of the mass fraction at every mesh node from the average mass fraction [42] or using the cell area weighted method [41]. Here, since the meshes vary as the cams rotate, the latter method was chosen and the calculation is given as:

$$\sigma^2 = \frac{\Sigma_{i=1}^{n} A_j (f_{1j} - f_{avg})^2}{A} \tag{5}$$

where A_j is the area of jth cell, A is the total area of the whole computational domain, n is the total number of cells in the whole computational domain, f_{1j} denotes the mass fraction of Liquid 1 in the jth cell, and f_{avg} is the mean mass fraction of Liquid 1 in the whole computational domain. As noted, Liquid 1 and 2 occupy the left and right cylinders, respectively, under the initial conditions, so f_{avg}=0.5 throughout the course of simulations.

To qualify the efficiency of mass transfer between the two cylinders, the mean mass fraction of Liquid 1 in the left cylinder (f_{lavg}) was employed and given as:

$$f_{lavg} = \frac{\Sigma_{k=1}^{m} A_k f_{1k}}{A_l} \tag{6}$$

where A_k is the area of the kth cell in the computational domain of the left cylinder (hereinafter referred to as "the left domain" for short), A_l is the total area of the left domain, m is the total number of cells in the left domain, f_{1k} denotes the mass fraction of Liquid 1 in the kth cell of the left domain.

In the laminar regime, stretch is a key operation to promote mixing [43]. The length stretch (β) is a normalized parameter to estimate the extent of stretch and defined as:

$$\beta = \frac{l_t}{l_0} \tag{7}$$

where l_t is the length of interface between two fluids at time t, and l_0 denotes the initial length of interface. In the following investigation, the interface is located where the mass fraction of Liquid 1 is 0.5 and l_0=36 mm (see Fig. 2).

MIXING RESULTS

In this section, the results of the 2D simulation of the mixing process in a TCM equipped with isosceles triangular cams are presented. Firstly, some flow simulations are presented and employed to discuss the mixing mechanism. Secondly, the impact of cam height-base ratio and eccentricity on the mixing process is illustrated. Finally, a relationship between the mixing performance and a dimensionless parameter determined by r and e is given.

1. Mixing Mechanism

To determine the mixing mechanism in a TCM with triangular cams, the mixing progress at the early stage when the interface between Liquid 1 and 2 is clear should be investigated. In this work, the geometric parameters of TCM are identical to those in the mesh independence test (see Table 1).

Fig. 6 presents the mixing process in TCM from 0 to 5/12 revolutions of the cams. At N=0, the two liquids are segregated left and right with a clear interface. With the rotation of the cams, the

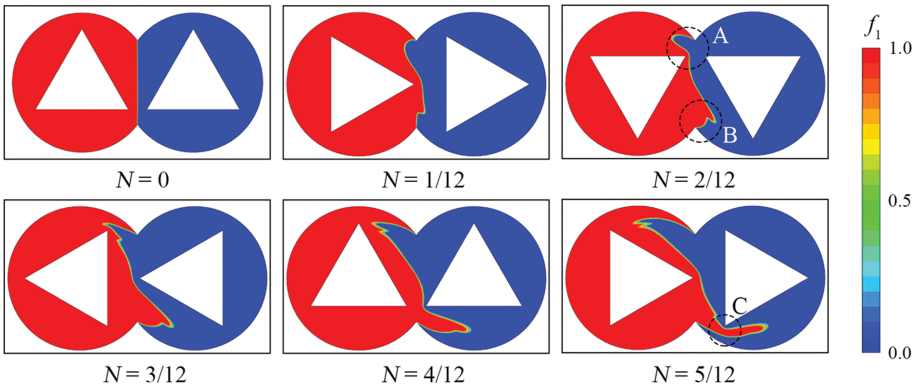


Fig. 6. Mass fraction contours of Liquid 1 for 0-5/12 revolutions of the cams (r=0.866, e=0).

interface becomes curved and obviously longer when N=1/12. As the cams rotate for 2/12 revolutions, two convex-shaped structures are separately located at A and B, indicating macroscopic mass transfer existed between the two cylinders. Liquid 1 is transported from the B to the right cylinder, while Liquid 2 is transported in reverse from A to the left cylinder. As the rotation of the cams continues, due to the distinct difference between velocity of fluids near the tips of the cams and the internal wall of the cavity, the two convex-shaped structures are stretched out to two sharp angles at N=3/12. Then, at N=4/12, the two sharp angles continue to be stretched longer and turn into two strips. In addition, the upper side of the strip below is disturbed by the left bottom tip of the right cam and becomes concave. As the cams keep rotating, at N=5/12, the strip above is further stretched, whereas the strip below becomes gradually narrower and is being folded at C. The mixing process in a TCM with triangular cams is basically dominated by three primary mixing mechanisms: macroscopic mass transfer between the two cylinders, stretch and fold.

A thorough study on the causes inducing the three primary mixing mechanisms was conducted here. The flow path lines are colored by the magnitude of velocity (u) at different revolutions of the cams are obtained in Fig. 7. As expected, the velocity of the fluid near the cams, especially the tips of the cams, is greater than that of the fluid near the internal wall of the cavity. In all results, some flow path lines colored by green, which corresponds to a velocity of 0.6 mm/s, run through the whole mixer along the inner wall of the cavity, which contributes to the macroscopic mass transfer between the two cylinders as described above. Furthermore, several vortexes caused by large velocity gradients can be observed near all the tips of the cams. The vortexes, which are also called secondary flows, can lead to the stretch and reorientation of the interface [41] as demonstrated in Fig. 6, which will further enhance the mass transfer between the two liquids. The stationary points in the flow field are among the most important features to investigate the dynamical behavior of fluids. The stationary points are defined by a zero velocity of the fluid [44] and the fluid near stationary points has a reduced velocity [5]. As shown Fig. 7, the stationary points are marked with black solid dots. At N=2/12 or 4/12, there is a stationary point at the center of the mixer, but at N=1/12 or 3/12, there are two stationary points near the center of the mixer. The cause for this phenomenon is that when a tip of either cam appears at the center of the mixer, it and its adjacent vortex will divide the stationary point into two and keep them away from the center of the mixer, which, to some extent, will avoid the formation of the dead zone.

2. Effects of Cam Height-base Ratio

To investigate the impact of the cam height-base ratio (r) on the mixing process in a TCM with triangular cams, the eccentricity (e) was kept constant and set to 0. The simulation results with r varying from 0.7 to 1.4 at an interval of 0.1 were compared with those obtained in the mesh independence test with r=0.866 and e=0. To compare the mixing processes fairly, all the simulations were terminated when the revolutions of the cams (N) reached 10.

Instantaneous mass fraction distributions of Liquid 1 with r=0.7, 0.866 and 1.4 are shown in Fig. 8. In all simulations, Liquid 1 and 2 were initially segregated in the left and right cylinders, respectively. The mass fraction distributions at N=0 are therefore not given here. At N=1/3, in all the three cases, Liquid 2 moves to the left cylinder through the middle-upper part of the cavity while Liquid 1 moves to the right cylinder by the middle-lower part of the cavity, enabling the exchange of liquids between the two cylinders. However, with r=1.4, the exchange is significantly more intense than that in the other two cases. This is probably attributable to different sweep ranges of the cams, and the cams with r=1.4 have distinctly larger radial sizes in comparison with those with r=0.7 or 0.866. At N=2/3, the mass transfer between the two cylinders is further increased. With r=1.4, Liquid 2 begins to occupy the lower part of the left cylinder, and conversely, Liquid 1 starts to fill the upper part of the right cylinder. However, with r=0.7 or 0.866, Liquid 2 only reaches the upper left part of the left cylinder and is squashed into a shuttle-shaped region, and at the same time, Liquid 1 is stretched into a striation at the lower right part of the right

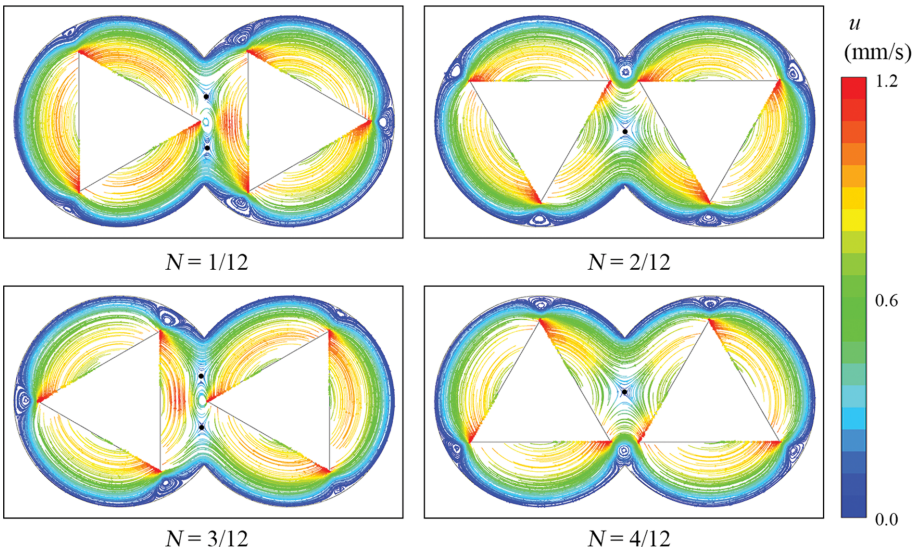


Fig. 7. Flow pattern for 1/12-4/12 revolutions of the cams (r=0.866, e=0).

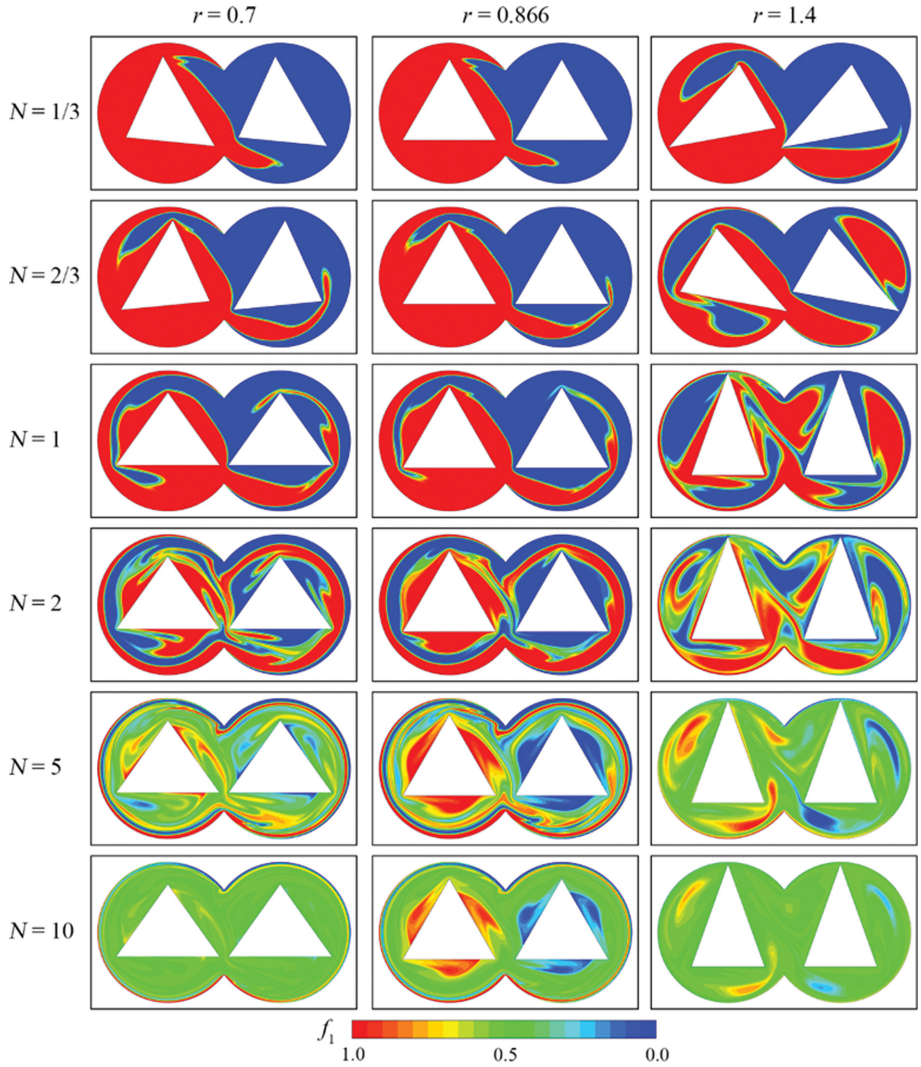


Fig. 8. Mass fraction evolution of Liquid 1 with different height-base ratios at e=0.

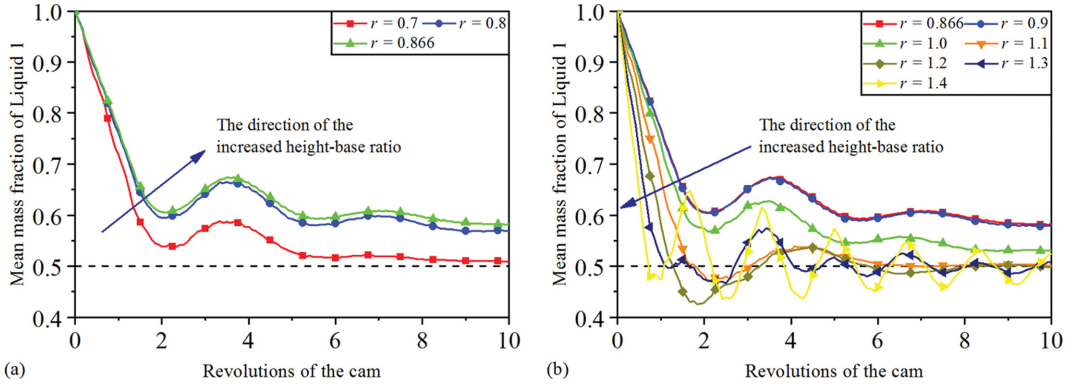


Fig. 9. Effects of height-base ratio on the mean mass fraction of Liquid 1 in the left cylinder at e=0 ((a) r varies from 0.7 to 0.866, (b) r varies from 0.866 to 1.4).

cylinder. In addition, slightly more liquids are transported with r=0.7 than those with r=0.866. At N=1, with r=1.4, some of Liquid 1 transported to the right cylinder returns to the left one, whereas some of Liquid 2 transported to the left cylinder goes back to the right one, which induces the circulation of the two liquids in the mixer. Besides, the interfaces between the two liquids begin to interact with each other. With r=0.7 or 0.866, the liquids transported to the other of the two cylinders are stretched into narrow

striations, which is conducive to mixing. At N=2, interaction among the interfaces takes place with r=0.7 and 0.866, but partial mixing can be observed with r=1.4, which might be caused by the continuous interaction of interfaces. As N=5, noticeable mixing can be found with r=0.7 and 1.4, whereas isolated regions can be found adjacent to all sides of the cams with r=0.866. When N is up to 10, non-uniform regions exist in spite of further mixing for all simulations. With r=0.7 and 0.866, the liquid near internal wall of the cavity is almost unmixed due to the large gap between the cams and the internal wall of the cavity. In addition, with r=0.866, the mass fraction distribution at the isolated regions is nearly the same as before. With r=1.4, there are four regions of inconsistent mass fraction distribution near the two cams, because the large radial sizes of the cams lead to the extremely small gap between the cams and the internal wall of the cavity and might dampen the mass transfer of liquid on both sides of the cams.

Fig. 9 presents the variations of the mean mass fraction of Liquid 1 in the left cylinder (f_{lavg}) regarding the revolutions of the cams (N) with different r. For a constant r, f_{lavg} decreases rapidly along with the increase of N in the initial stage. Then, f_{lavg} starts to fluctuate around a constant value and the amplitude of the fluctuation decreases gradually, rotation of the cam continues. The fluctuation is caused by the cycling of the unmixed liquid in the mixer. When part of unmixed Liquid 1 moves from the left cylinder to the right one, f_{lavg} decreases from the maximum to the minimum. When part of unmixed Liquid 1 moves from the right cylinder to the left one, f_{lavg} increases from the minimum to the maximum. The greater the deviation between r and 0.866 is, the more drastic is the fluctuation and thereby the stronger is the macroscopic mass transfer between the two cylinders. In addition, the greater the deviation between r and 0.866 is, the faster the is decline of f_{lavg} is at the beginning. As r varies from 0.7 to 1.0, the closer r is to 0.866, the higher the value f_{lavg} fluctuates around is due to the isolated regions adjacent to the sides of the cams noted before. With r=0.866, f_{lavg} fluctuates around 0.6, which is higher than that of all other cases.

A plot showing the variation of the length stretch (β) which is dependent on the revolutions of the cams when r=0.7 and e=0 is presented in Fig. 10. Obviously, β initially increases along with the increase of the revolutions of the cams (N). Approximately after N=1.3, β fluctuates irregularly but maintains an upward trend on

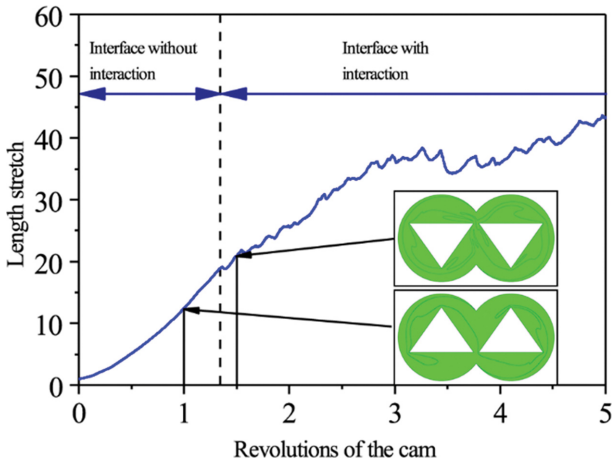


Fig. 10. Variation of the length stretch with respect to the revolutions of the cams (r=0.7, e=0).

the whole. The reason behind the phenomenon is that there is no interaction among the interfaces before N=1.3 and the interaction of the interfaces takes place after N=1.3. In the plot, the interface without and with interaction in TCM can be observed at N=1 and 1.5, respectively.

Fig. 11 shows the variations of β with different r and N in the range of 0 to 1, which is sufficient to determine the efficiency of stretching in the mixer. In all cases, β generally increases as N increases from 0 to 1. However, with r=1.4, β suddenly decreases when N approaches to 1 due to the interaction of the interfaces, which agrees with the observation in Fig. 8. As shown in both Figs. 11(a) and (b), the closer r is to 0.866, the more slowly β increases, thus the lower is the efficiency of stretching.

The mixing quality (α) with respect to the revolutions of the cams (N) at different r is plotted in Fig. 12. As can be anticipated, with a given r, α rises relatively fast at the beginning and then the upward trend slows. At a constant N, α generally increases with the increase in the deviation between r and 0.866. However, α with r=1.4 is lower than that with r=1.2 and 1.3 when N>5, which might be caused by the large radial size of the cams dampening the mass transfer of liquid on both sides of the cams. In addition, α reaches the maximum, that is, approximately 0.9, with r=1.3 and N=10. In summary, the cam height-base ratio (r) has consid-

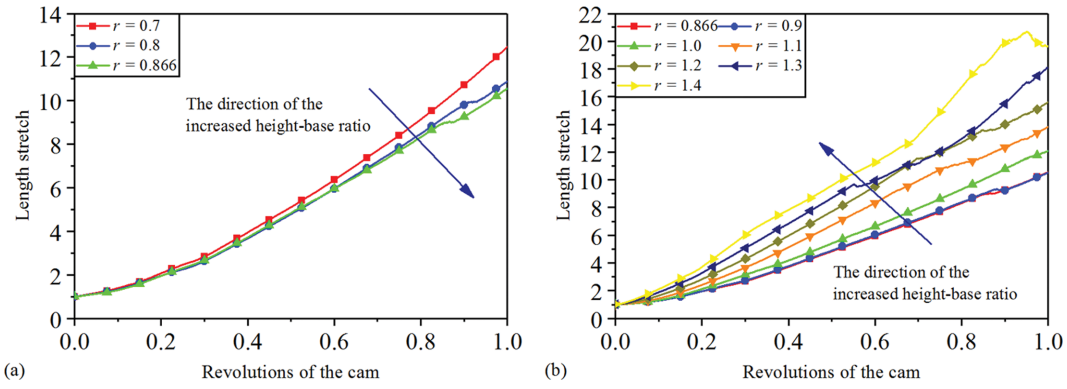


Fig. 11. Effect of height-base ratio on the length stretch at e=0 ((a) r varies from 0.7 to 0.866, (b) r varies from 0.866 to 1.4).

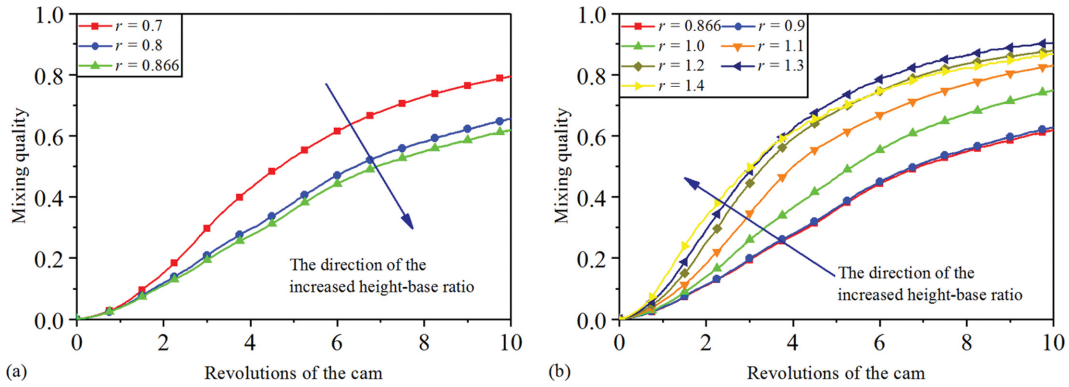


Fig. 12. Effect of height-base ratio on the mixing quality at e=0 ((a) r varies from 0.7 to 0.866, (b) r varies from 0.866 to 1.4).

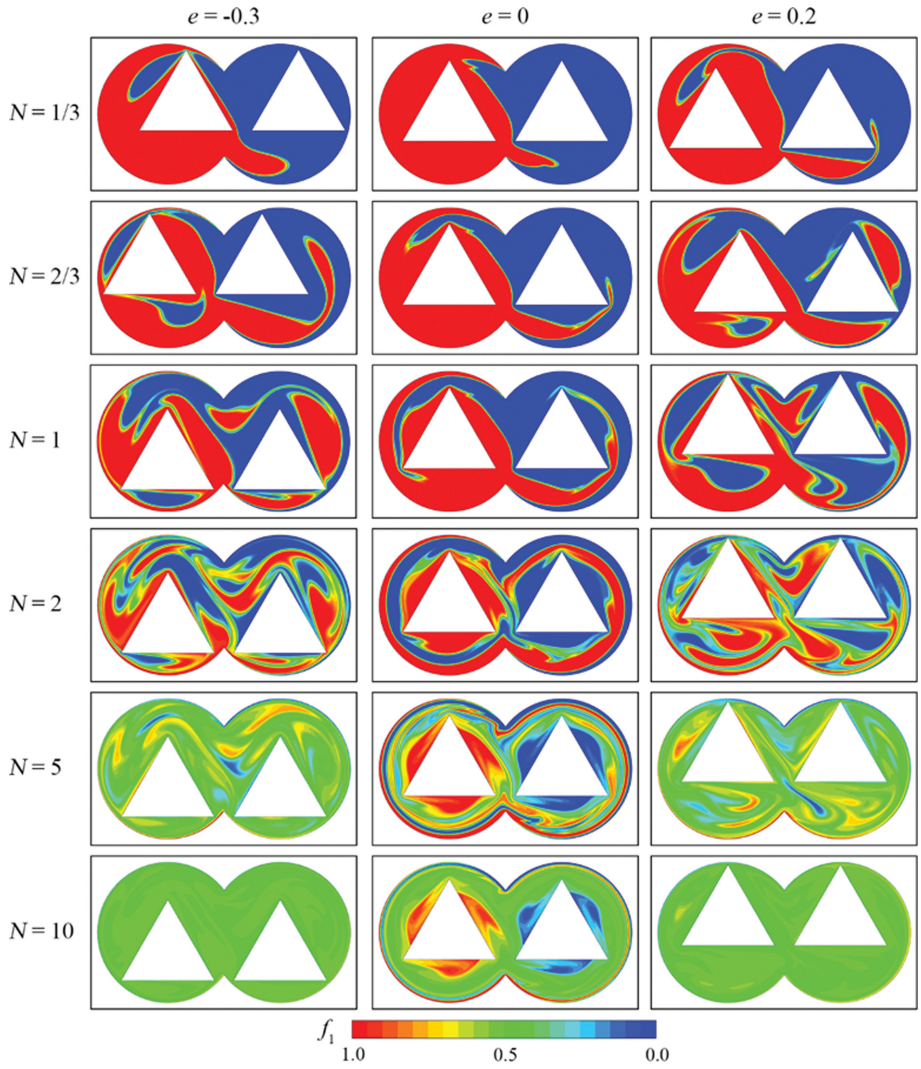


Fig. 13. Mass fraction evolution of Liquid 1 with different eccentricity at r=0.866.

erable influence on the mass fraction distribution, length stretch and mixing quality thereby affecting the performance of TCM.

3. Effects of Cam Eccentricity

In this section, the effects of the cam eccentricity (e) on the mixing process in TCM are studied. In all cases investigated here, the height-base ratio (r) was kept as 0.866 (as a result of the equilateral triangular cams). The simulation results with e varying from −0.3 to 0.2 at an interval of 0.05 were obtained and all the simulations also terminated at N=10.

Instantaneous mass fraction distributions of Liquid 1 with e=

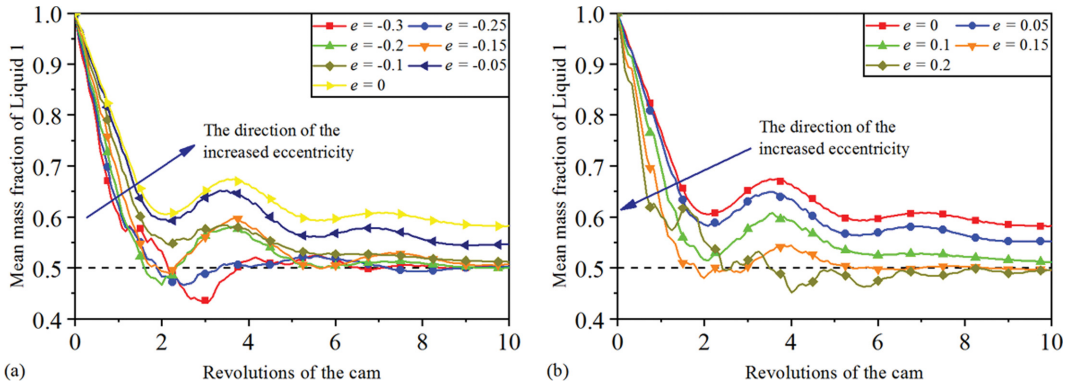


Fig. 14. Effects of eccentricity on the mean mass fraction of Liquid 1 in the left cylinder with r=0.866 ((a) e varies from −0.3 to 0, (b) e varies from 0 to 0.2).

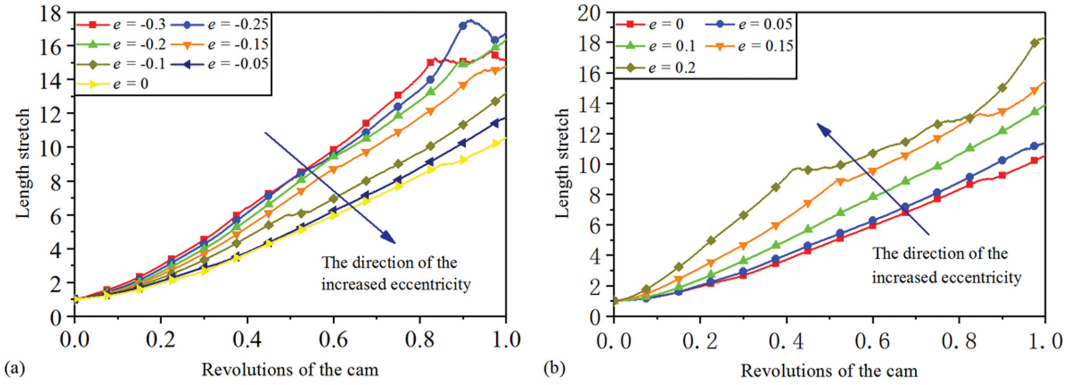


Fig. 15. Effect of eccentricity on the length stretch at r=0.866 ((a) e varies from −0.3 to 0, (b) e varies from 0 to 0.2).

−0.3, 0 and 0.2 are shown in Fig. 13. At N=1/3 to 1, the exchange of liquids between the two cylinders with e=−0.3 and 0.2 is noticeably more than that with e=0. Moreover, at N=1, the interfaces in the mixer with e=−0.3 or 0.2 have interacted with each other, while the interaction of the interfaces does not occur yet with e=0. At N=2 to 10, for all simulations, mass fraction distributions of Liquid 1 become increasingly homogeneous, and the mixing rates with e=−0.3 and 0.2 are significantly higher than that with e=0. Furthermore, at N=10, the heterogeneous regions in the mixer with e=−0.3 or 0.2 have almost disappeared, whereas this is not the case with e=0.

Fig. 14 shows the variation of the mean mass fraction of Liquid 1 in the left cylinder (f_{lavg}) with respect to the revolutions of the cams (N) with different *e*. For a given e, f_{lavg} decreases sharply with the increase in N at the beginning. Subsequently, f_{lavg} begins to fluctuate around a certain value and the amplitude of fluctuation decreases gradually as the rotation of the cams goes on. The fluctuation is also due to the circulation of the unmixed liquid in the mixer as mentioned above. However, the amplitude of fluctuations in all cases is similar; thus *e* has little effect on the fluctuation of f_{lavg}. The greater the deviation between e and 0 is, the faster is the decrease of f_{lavg} at the beginning. With e=−0.05, 0 and 0.05, the value that f_{lavg} fluctuates around is larger than 0.5 due to the isolated regions mentioned before. Especially, with e=0, f_{lavg} fluctuates around 0.6, which is the highest in all cases.

Fig. 15 presents the variation of β with different e and N varying from 0 to 1. In all cases, β generally increases with the increase of N from 0 to 1. However, when e is 0.2, 0.15 or varies from −0.3 to −0.15, the fluctuation of β occurs before N=1 due to the interaction of interfaces. The closer e is to 0, the more slowly β increases, thus the lower the efficiency of stretching is.

The mixing quality (α) with respect to the revolutions of the cams (N) with different e is illustrated in Fig. 16. As expected, for a given e, α rises rapidly in the initial stage, and then the upward trend slows. At a constant N, α generally increases with the increase in the deviation between e and 0. In addition, when e=−0.3 and N=10, α is around 0.95, which is closest to 1 among all simulations here. Accordingly, the cam eccentricity (e) also has significant effect on the performance of TCM.

4. Geometry Quantification of TCM

To characterize the rotor in a continuous mixer, Manas-Zloczower and Tadmor [45] proposed a dimensionless parameter called the pressurization coefficient (S):

$$S = \frac{\left(1-\frac{h_0}{H_0}\right)^2}{1+2\frac{c}{h}\tan\theta-\left(\frac{h_0}{H_0}\right)^2} \tag{8}$$

where θ, c, h_0, and H_0 refer to the leading face angle, the tip width, the minimum and maximum clearances between the rotor and

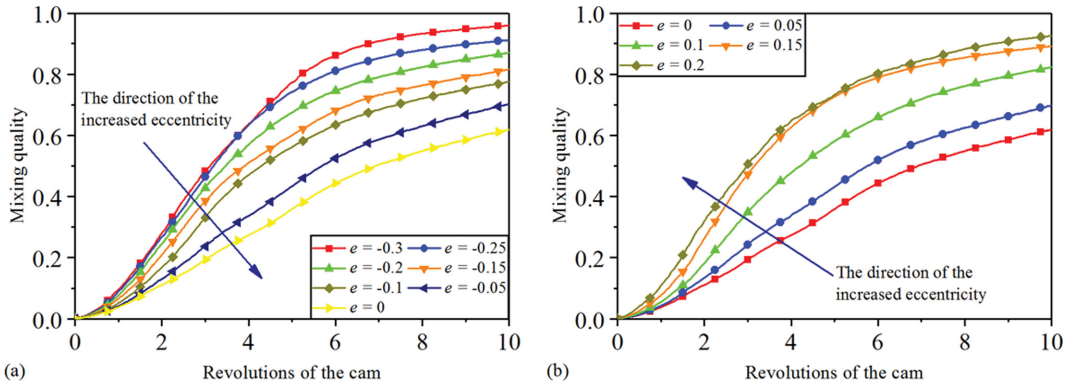


Fig. 16. Effect of eccentricity on the mixing quality at r=0.866 ((a) e varies from −0.3 to 0, (b) e varies from 0 to 0.2).

the inner wall of cavity, respectively. The derivation process of Eq. (8) can be seen in Ref. [45]. The larger S is, the more materials will undergo the shear and elongational flow near the cam tips, which is conducive to dispersive mixing [11].

In a continuous mixer, the rotor usually consists of two identical wing tips; it is sufficient to consider only one tip in implementing the geometry quantification of the rotor. However, the three tips of a triangular cam are probably not the same, so all the three tips should be taken into consideration. Since a larger S indicates a stronger mixing ability [11], the maximum of three pressurization coefficients corresponding to three tips is obtained to quantify the triangular cam in a TCM. Furthermore, note that the tip width of the triangular cam is 0, so the middle term of the denominator in Eq. (8) is removed here. On this basis, the modified pressurization coefficient (S_m) used for the triangular cam is defined as:

$$S_m = \max\left\{\frac{1-\frac{h_1}{H_1}}{1+\frac{h_1}{H_1}}, \frac{1-\frac{h_2}{H_2}}{1+\frac{h_2}{H_2}}, \frac{1-\frac{h_3}{H_3}}{1+\frac{h_3}{H_3}}\right\} \tag{9}$$

where h_1, h_2 and h_3 denote the clearance between the three tips and the inner wall of cavity, H_1, H_2 and H_3 refer to the maximum clearances between the inner wall of cavity and three leading faces (namely three sides of the cam) corresponding to three tips.

The modified pressurization coefficients (S_m) for all cases investigated in the previous two sections are calculated and presented in Fig. 17. When r and e are given, S_m can be determined. It can be found that the minimum S_m is obtained when r=0.866 and e=0. When r=0.866, the greater the deviation between e and 0 is, the larger is S_m. Similarly, when e=0, the greater the deviation between r and 0.866 is, the larger is S_m. Based on the conclusions of the previous two sections, it can be inferred that the larger S_m is, the better is the mixing performance, which agrees with Ref. [11]. To clearly determine the relationship between the modified pressurization coefficients (S_m) and the mixing performance of a TCM equipped with triangular cams, the mixing quality at N=10 ($\alpha_{N=10}$) for all cases studied in the previous two sections except that with r=1.4 and e=0 was obtained. As described in Section Effects of cam height-base ratio, the mixing quality (α) with r=1.4 and e=0 is not as good as theoretically predicted and there still exist unmixed regions at N=10 because the relatively large radial sizes of the cams might dampen mixing. The variation of $\alpha_{N=10}$ with respect to S_m is plotted in Fig. 18, in which the optimal structure with r=0.866 and e=−0.3 and the reference structure with r=0.866 and e=0 are marked. As expected, $\alpha_{N=10}$ generally increases with the

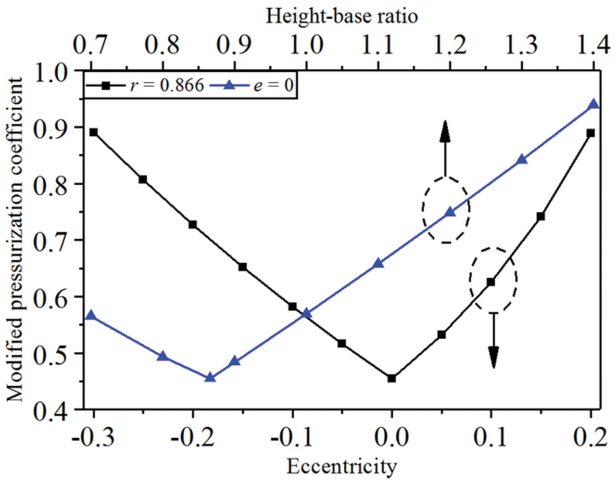


Fig. 17. Modified pressurization coefficient with respect to height-base ratio and eccentricity.

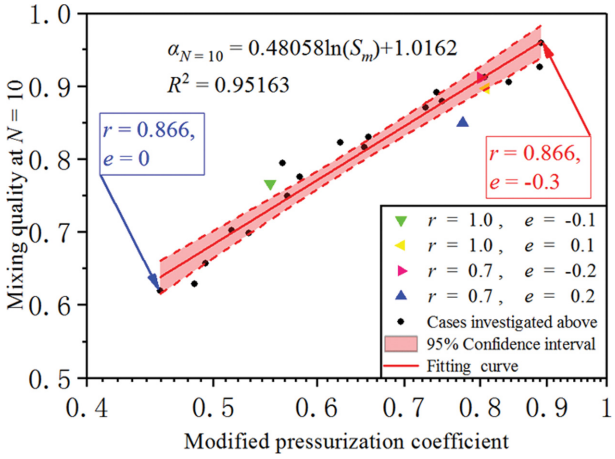


Fig. 18. Mixing quality at N=10 with respect to modified pressurization coefficient.

Table 3. The errors between simulation $\alpha_{N=10}$ and $\alpha_{N=10}$ predicted by the correlation

Cases	r	e	S_m	Simulation $\alpha_{N=10}$ (α_{sim})	$\alpha_{N=10}$ calculated by the correlation (α_{cal})	Errors ($\lvert\alpha_{sim}-\alpha_{cal}\rvert/\alpha_{sim}$)
1	1.0	−0.1	0.552	0.766	0.731	4.6%
2	1.0	0.1	0.808	0.896	0.914	2.0%
3	0.7	−0.2	0.800	0.911	0.909	0.2%
4	0.7	0.2	0.776	0.849	0.894	5.3%

increase in S_m. The following logarithmic form is achieved by nonlinear fitting of these data (see Fig. 18):

$$\alpha_{N=10}=0.48058\ln(S_m)+1.0162 \quad (10)$$

The coefficients of the correlation (Eq. (10)) are determined by the Levenberg-Marquardt (L-M) algorithm, which works well in most cases and serves as a standard to nonlinear least square routines. In addition, the 95% confidence interval of the correlation is also shown in Fig. 18.

To verify the applicability of Eq. (10), the results of S_m in four cases with r=1.0 and e=−0.1, r=1.0 and e=0.1, r=0.7 and e=−0.2, r=0.7 and e=0.2, respectively, were obtained and shown in Fig. 18. Data points corresponding to the four cases are near the fitting curve. In addition, the errors between simulated $\alpha_{N=10}$ (α_{sim}) and $\alpha_{N=10}$ calculated by the correlation (α_{cal}) in the four cases are listed in Table 3, which are close to or less than 5%. Therefore, the correlation can be used to predict the mixing performance in a TCM with two identical isosceles triangular cams. The correlation is applicable when a TCM works with a rotation speed of 0.5 rpm, a cam height-base ratio of 0.7-1.3, an eccentricity of −0.3-0.2, and two fluids with a viscosity of 50 Pa·s and a density of 1,500 kg/m^3 fully occupy the left and right cylinders, respectively, in the initial conditions.

CONCLUSIONS

The mixing process of two initially stratified miscible fluids in a 2D TCM with two identical isosceles triangular cams moving at 0.5 rpm was investigated through a verified 2D numerical model. This study shows that flow circulation running through the whole mixer along the inner wall of the cavity contributes to macroscopic mass transfer; several vortexes near all the tips of the cams leading to the stretch and reorientation of the interface were also observed. The influence of cam height-base ratio (r) and eccentricity (e) was studied. The qualitative and quantitative results both indicate that the two geometric parameters have a significant effect on the mixing behavior of the mixer. In general, the closer r is to 0.866 or e is to 0, the worse mixing performance a TCM has. A modified pressurization coefficient (S_m) determined by r and e was proposed, and a logarithmic relationship between the mixing quality (α) and S_m was discovered, which provides an idea for establishing the relationship between the geometric parameters of the mixer and its mixing performance. It is hoped that the validated computational methods and models could be used to simulate the mixing process of similar mixers with different conditions (e.g., a higher rotating speed, non-Newtonian fluids) in the future.

ACKNOWLEDGEMENTS

This project is supported by National Natural Science Foundation of China (Grant Nos. 51975226 and 51605179).

NOMENCLATURE

a : distance between the centers of the cavity cylinders [m]
A : total area of the whole computational domain [m^2]
A_j : area of jth cell [m^2]
A_k : area of kth cell in the computational domain of the left cavity cylinder [m^2]
A_l : total area of the left domain [m^2]
b : base of the cams [m]
c : tip width of cam [m]
d : diameters of the cavity cylinders [m]
D_m : mass diffusion coefficient [m^2/s]
e : ratio of E to the radius of the cavity cylinder
E : distance between the center of the cavity cylinder and the centroid of the cam at the same side [m]
f_{1j} : mass fraction of Liquid 1 in *j*th cell
f_{1k} : mass fraction of Liquid 1 in *k*th cell of the left domain
f_2 : mass fraction of Liquid 2
f_{avg} : mean mass fraction of Liquid 1 in whole computational domain
f_i : mass fraction of the species *i*
f_{lavg} : mean mass fraction of Liquid 1 in the left cavity cylinder
F : source term [N/m^3]
h : height of the cams [m]
h_0 : minimum clearances between the rotor and the cavity wall [m]
h_1, h_2, h_3 : clearance between the three tips and cavity wall [m]
H_0 : maximum clearances between the rotor and the cavity wall [m]
H_1, H_2 H_3 : maximum clearance between the cavity wall and three leading faces [m]
l_0 : initial length of the interface [m]
l_t : interfacial length between the two fluids at time t [m]
m : total number of cells in the left domain
n : total number of cells in computational domain
N : revolutions of the cam
p : fluid pressure [Pa]
P_d : centroid of the left cam
P_{cr} : centroid of the right cam
P_r : sampling point located at (0, 52 mm)
P_{rl} : center of left cavity cylinder

P_{rr} : center of left cavity cylinder
r : cam height-base ratio
S : pressurization coefficient
S_{cam} : cam area [m^2]
S_m : modified pressurization coefficient
t : time [s]
Δt : time step [s]
u : magnitude of velocity [m/s]
u : velocity vector [m/s]
Δx : mesh size [m]

Greek Letters

α : mixing quality
β : length stretch
θ : leading face angle
ρ : fluid density [kg/m^3]
σ^2 : variance of mass fraction distribution
σ^2_{max} : the maximum variance
τ : viscous stress tensor

REFERENCES

1. G. Grosso, M. A. Hulsen, A. S. Fard, A. Overend and P. D. Anderson, *AIChE J.*, **64**, 1034 (2018).
2. R. Wójtowicz and J. Talaga, *Chem. Eng. Commun.*, **203**, 161 (2016).
3. R. Wójtowicz, *Chem. Eng. Sci.*, **172**, 622 (2017).
4. Y. Li, J. Si, M. Arowo, Z. Liu, B. Sun, Y. Song, G. Chu and L. Shao, *Chem. Eng. Process. - Process Intensification*, **148**, 107801 (2020).
5. M. Robinson and P. W. Cleary, *AIChE J.*, **57**, 581 (2011).
6. T. Avalosse and M. J. Crochet, *AIChE J.*, **43**, 577 (1997).
7. F. Bertrand, F. Thibault, L. Delamare and P. A. Tanguy, *Comput. Chem. Eng.*, **27**, 491 (2003).
8. M. Robinson, P. Cleary and J. Monaghan, *AIChE J.*, **54**, 1987 (2008).
9. A. Eitzlmayr, G. Koscher and J. Khinast, *Comput. Phys. Commun.*, **185**, 2436 (2014).
10. J. Liu, F. Li, L. Zhang and H. Yang, *J. Appl. Polym. Sci.*, **132**, 42496 (2015).
11. T. Chen, Y. Hao, X. Chen, H. Zhao, J. Sha, Y. Ma and L. Xie, *J. Appl. Polym. Sci.*, **135**, 46623 (2018).
12. Y. Nakayama, T. Kajiwara and T. Masaki, *AIChE J.*, **62**, 2563 (2016).
13. S. A. Salahudeen, R. H. Elleithy, O. AlOthman and S. M. AlZahrani, *Chem. Eng. Sci.*, **66**, 2502 (2011).
14. J. Luo, B. Xu, H. Yu, Y. Du and Y. Feng, *Fiber. Polym.*, **16**, 95 (2015).
15. B. Xu, Y. Liu, H. Yu, L. Turng and C. Liu, *Macromol. Theor. Simul.*, **27**, 1800021 (2018).
16. H. H. Yang and I. Manas-Zloczower, *Polym. Eng. Sci.*, **32**, 1411 (1992).
17. X. Zhang, L. Feng, W. Chen and G. Hu, *Polym. Eng. Sci.*, **49**, 1772 (2009).
18. A. S. Fard and P. D. Anderson, *Comput. Fluids*, **87**, 79 (2013).
19. T. Ishikawa, F. Nagano, T. Kajiwara and K. Funatsu, *Int. Polym. Proc.*, **21**, 354 (2006).
20. Y. Nakayama, E. Takeda, T. Shigeishi, H. Tomiyama and T. Kajiwara, *Chem. Eng. Sci.*, **66**, 103 (2011).
21. Y. Nakayama, H. Takemitsu, T. Kajiwara, K. Kimura, T. Takeuchi and H. Tomiyama, *AIChE J.*, **64**, 1424 (2018).
22. O. S. Carneiro, G. Caldeira and J. A. Covas, *J. Mater. Process. Tech.*, **92**, 309 (1999).
23. X. Zhang, Z. Xu, L. Feng, X. Song and G. Hu, *Polym. Eng. Sci.*, **46**, 510 (2006).
24. X. Zhang, L. Feng, S. Hoppe and G. Hu, *Polym. Eng. Sci.*, **48**, 19 (2008).
25. G. Shearer and C. Tzoganakis, *Polym. Eng. Sci.*, **39**, 1584 (1999).
26. G. Shearer and C. Tzoganakis, *Polym. Eng. Sci.*, **40**, 1095 (2000).
27. G. Shearer and C. Tzoganakis, *Adv. Polym. Technol.: J. Polym. Process. Inst.*, **20**, 169 (2001).
28. G. Shearer and C. Tzoganakis, *Polym. Eng. Sci.*, **41**, 2206 (2001).
29. X. Zhan, Z. Sun, Y. He, B. Shen, T. Shi and X. Li, *Can. J. Chem. Eng.*, **97**, 1931 (2019).
30. F. Huang, D. Wang, Z. Li, Z. Gao and J. J. Derksen, *Chem. Eng. J.*, **362**, 229 (2019).
31. C. Park, K. Lee, S. Hong, J. Lee, S. Cho and I. Moon, *Powder Technol.*, **355**, 309 (2019).
32. M. Mansour, Z. Liu, G. Janiga, K. D. P. Nigam, K. Sundmacher, D. Thévenin and K. Zähringer, *Chem. Eng. Sci.*, **172**, 250 (2017).
33. R. K. Connelly and J. L. Kokini, *Adv. Polym. Technol.*, **22**, 22 (2003).
34. R. K. Connelly and J. L. Kokini, *J. Non-Newton. Fluid*, **123**, 1 (2004).
35. R. K. Connelly and J. L. Kokini, *J. Food Eng.*, **79**, 956 (2007).
36. Q. He, J. Huang, X. Shi, X. Wang and C. Bi, *Comput. Math. Appl.*, **73**, 109 (2017).
37. J. Cheng and I. Manas-Zloczower, *Polym. Eng. Sci.*, **29**, 701 (1989).
38. R. B. Bird, R. C. Armstrong and O. Hassager, *Dynamics of polymeric liquids*, Wiley, New York (1987).
39. P. Dhakal, S. R. Das, H. Poudyal and A. J. Chandy, *J. Appl. Polym. Sci.*, **134**, 44250 (2017).
40. ANSYS, ANSYS Fluent User's guide, release 19.0 (2017).
41. U. Fatima, M. Shakaib and I. Memon, *Chem. Pap.*, **74**, 1267 (2020).
42. P. Vatankhah and A. Shamloo, *Anal. Chim. Acta*, **1022**, 96 (2018).
43. J. M. Ottino, *The kinematics of mixing: stretching, chaos, and transport*, Cambridge University Press, New York (1989).
44. S. Smale, *B. Am. Math. Soc.*, **73**, 747 (1967).
45. I. Manas-Zloczower and Z. Tadmor, *Mixing and compounding-theory and practice*, Hanser, Cincinnati (2009).